Static and dynamical spin correlations of the $S=\frac{1}{2}$ random-bond antiferromagnetic Heisenberg model on the triangular and kagome lattices

Tokuro Shimokawa,* Ken Watanabe, and Hikaru Kawamura
Department of Earth and Space Science, Graduate School of Science, Osaka University, Toyonaka, Osaka 560-0043, Japan
(Received 11 June 2015; revised manuscript received 2 September 2015; published 9 October 2015)

Inspired by the recent theoretical suggestion that the random-bond $S = 1/2$ antiferromagnetic Heisenberg model on the triangular and the kagome lattices might exhibit a randomness-induced quantum spin liquid (QSL) behavior when the strength of the randomness exceeds a critical value, and that this "random-singlet state" might be relevant to the QSL behaviors experimentally observed in triangular organic salts κ-$(ET)_2Cu_2(CN)_3$ and $EtMe_3Sb[Pd(dmit)_2]_2$ and in kagome herbertsmithite $ZnCu_3(OH)_6Cl_2$, we further investigate the nature of the static and the dynamical spin correlations of these models. We compute the static and the dynamical spin structure factors, $S(\mathbf{q})$ and $S(\mathbf{q},\omega)$, by means of an exact diagonalization method. In both triangular and kagome models, the computed $S(\mathbf{q},\omega)$ in the random-singlet state depends on the wave vector $\mathbf{q}$ only weakly, robustly exhibiting gapless behaviors accompanied by the broad distribution extending to higher energy ω. Especially in the strongly random kagome model, $S(\mathbf{q},\omega)$ hardly depends on $\mathbf{q}$, and exhibits an almost flat distribution for a wide range of ω, together with a $\omega = 0$ peak. These features agree semiquantitatively with the recent neutron-scattering data on a single-crystal herbertsmithite. Furthermore, the computed magnetization curve agrees almost quantitatively with the experimental one recently measured on a single-crystal herbertsmithite. These results suggest that the QSL state observed in herbertsmithite might indeed be the randomness-induced QSL state, i.e., the random-singlet state.

DOI: 10.1103/PhysRevB.92.134407 PACS number(s): 75.10.Jm, 75.10.Kt, 75.10.Nr

I. INTRODUCTION

Geometrically frustrated magnets have attracted a long-standing and ongoing attention in the field of condensed matter physics because they often give rise to a variety of nontrivial thermodynamic states. In particular, the quantum spin liquid (QSL) state having no magnetic long-range order (LRO) has been extensively investigated both theoretically and experimentally. Anderson proposed the resonating valence bond (RVB) state as a possible ground state of the $S = 1/2$ Heisenberg antiferromagnet on the triangular lattice [1]. According to many subsequent theoretical studies, however, it is now widely believed that the ground state of a simple $S = 1/2$ antiferromagnetic (AF) Heisenberg model on the triangular lattice with the nearest-neighbor bilinear interaction exhibits a Néel LRO with the three-sublattice 120° structure [2–4].

By contrast, the ground state of the $S = 1/2$ Heisenberg model on the kagome lattice, which has stronger frustration than the triangular lattice, is quite likely to be nonmagnetic. Namely, the absence of the magnetic LRO in the $S = 1/2$ kagome AF Heisenberg model has now been established from various numerical studies [5–21], although the precise nature of its ground state still remains controversial. Various candidates, including the gapped Z_2 spin-liquid [17,18,22,23], the gapless U(1) spin liquid [15,24–27], the chiral spin liquid [28], and the valence bond crystal [11,29,30], etc., have been proposed.

Along with these theoretical studies, experimental quest for the QSL has also been persued. As a result, several promising candidate materials were recently reported. In the triangular system, certain organic salts such as κ-$(ET)_2Cu_2(CN)_3$ [31–43] and $EtMe_3Sb[Pd(dmit)_2]_2$ [44–49] were reported to exhibit a QSL-like behavior, i.e., exhibit no magnetic LRO down to a very low temperature. These organic materials show gapless (or nearly gapless) behaviors at low temperatures. For example, the specific heat [35,47] and the thermal conductivity [36,46] exhibit a behavior linear in the absolute temperature T. Obviously, in understanding the QSL-like properties of these triangular organic salts, some extension beyond the simplest nearest-neighbor Heisenberg model is needed [50–57].

In the kagome system, herbertsmithite $ZnCu_3(OH)_6Cl_2$ was reported to be a candidate of QSL, again showing gapless behaviors in various physical quantities [58–65]. The true nature of these gapless QSL candidates experimentally observed both in the triangular and kagome lattice AFs has still remained obscure in spite of much theoretical and experimental efforts devoted to the issue.

For years, major part of theories have tried to elucidate the experimentally observed QSL behaviors as properties of a clean and regular system. By contrast, it was proposed recently in Refs. [66,67] that the quenched bond-randomness, together with the geometrical frustration effect, might be essential in stabilizing the experimentally observed gapless QSL state both in the triangular organic salts and in the kagome herbersmithite. Such a randomness-induced QSL state is called the "random-singlet state" [68–71] or the "valence bond glass state" [72,73], where the spin singlet is formed in a spatially random manner. The possible importance of the quenched site randomness in kagome herbertsmithite was also pointed out in Ref. [73].

The origin or even the existence of the quenched randomness in triangular organic salts and kagome herbertsmithite is a nontrivial matter, especially in view of the fact that the theory requires a considerable amount of randomness, not an infinitesimal one, to realize the QSL-like behavior [66,67]. In the case of the triangular organic salts, it was suggested

*Corresponding author: t.shimokaw@gmail.com

that the randomness for the spin degrees of freedom was self-generated at low temperatures via the random freezing of the electric-polarization degrees of freedom inherent to these organic salts consisting of molecular dimers [66]. In fact, the measured ac dielectric constant of these organic salts exhibited a glassy response even on a macroscopic time scale of kilohertz in the temperature region where the QSL behavior was observed in the spin degree of freedom [38].

In the case of kagome herbertsmithite, the quenched randomness comes from the random substitution of nonmagnetic Zn^{2+} by magnetic Cu^{2+}, located on the triangular layer adjacent to the kagome layer [63,67]. Note that the kagome layers in herbertsmithite are separated by $[Zn(OH)_6]^{4-}$ octahedral units whose Zn^{2+} constitutes the triangular layer. It was reported that about 15% of Zn^{2+} on the triangular layer was randomly substituted by Cu^{2+}, keeping the kagome layer intact [63]. Since Cu^{2+} is a Jahn-Teller ion, such a random substitution would lead to a random Jahn-Teller distortion of the $[Cu(OH)_6]^{4-}$ octahedra, leading to the random modification of the exchange path, and subsequently the exchange strength, connecting the Cu^{2+} on the kagome layer [74].

Indeed, the numerical results on a simplified random $S = 1/2$ AF Heisenberg model on the triangular and the kagome lattices appear to reproduce many of experimentally observed features [66,67] of various thermodynamic quantities, including the T-lienar low-temperature specific heat [35,47,59], the gapless magnetic susceptibility occasionally accompanying a Curie-like tail [62], and the gapless temperature dependence of the NMR relaxation rate $1/T_1$ [33,45].

In view of this apparent success of the random model in reproducing the experimentally observed QSL-like behaviors, it would be desirable to further investigate the nature of the static and the dynamical spin correlations of the randomness-induced QSL state, the random singlet state. For this purpose, in the present paper we compute by means of an exact diagonalization technique the static and the dynamical spin structure factors which are experimentally accessible via, e.g., the elastic and the inelastic neutron scattering measurements. Such a comparison between theory and experiment might give further information in examining the validity of the randomness-induced QSL picture of the experimentally observed QSL states. In order to clarify the effect of frustration, we perform comparative calculations also on the random-bond $S = 1/2$ AF Heisenberg model on the square lattice.

Our numerical results corroborates the previous observation that both the triangular and the kagome models exhibit the randomness-induced QSL-like behavior when the randomness exceeds a critical value [66,67]. Meanwhile, the unfrustrated square model persistently exhibits the AF LRO up to the maximal randomness without showing the QSL-like behavior. The result highlights an important role of frustration, along with the randomness and the quantum fluctuation, in stabilizing the random-singlet state.

The random-singlet states in the triangular and kagome models have some mutual similarities, but also some differences. In the triangular case, the random-singlet state keeps a certain amount of AF short-range order even at the maximal randomness. While the dynamical structure factor $S(\mathbf{q},\omega)$ of the triangular model exhibits a signature of the AF LRO and the magnon excitation in the regular and weakly random cases, in the strongly random case corresponding to the random-singlet state, it exhibits a gapless behavior accompanied by a broad ω distribution extending to higher energy, which is dependent on the wave vector $\mathbf{q}$ only weakly. In the kagome case, by contrast, a signature of the AF LRO or the magnon excitation is hardly discernible either in the regular or in the random case. Peaky features of $S(\mathbf{q},\omega)$ still retained in the regular case give way to gapless behaviors in the strongly random case corresponding to the random singlet state. Such features of $S(\mathbf{q},\omega)$ are accompanied by an almost flat distribution in a wide range of ω and by an $\omega = 0$ peak, which hardly depends on the wave vector $\mathbf{q}$. Indeed, these features of the computed $S(\mathbf{q},\omega)$ of the strongly random kagome model are compared quite favorably with the recent inelastic-neutron scattering data on a single-crystal kagome herbersmithite [64].

This paper is organized as follows. In Sec. II, we present our model and the details of our numerical calculation. In Secs. III and IV, we show the results of our numerical calculations in the case of the triangular and the kagome models, respectively. Section V is devoted to summary and discussion. For comparison, we also present the corresponding results for the unfrustrated square-lattice model in Appendix A. The detailed information about the shape of finite-size lattices employed in our exact-diagonalization calculation is given in Appendix B.

II. THE MODEL AND THE METHOD

Our model is the AF random-bond $S = 1/2$ quantum Heisenberg model on the triangular and the kagome lattices, whose Hamiltonian is given by

$$\mathcal{H} = \sum_{i,j} J_{i,j}\mathbf{S}_i \cdot \mathbf{S}_j, \tag{1}$$

where $\mathbf{S}_i = (S_i^x, S_i^y, S_i^z)$ is a spin-1/2 operator at the ith site on the lattice, while $J_{i,j} > 0$ is the random nearest-neighbor AF coupling obeying the bond-independent uniform distribution between $[(1-\Delta)J,(1+\Delta)J]$ with the mean J. The parameter Δ represents the extent of the randomness: $\Delta = 0$ and $\Delta = 1$ cases correspond to the regular and maximally random cases, respectively.

According to Refs. [66,67], the random-singlet ground state is realized when the randomness is stronger than a critical value Δ_c. In the triangular model, Δ_c is estimated to be $\simeq 0.6$ where Δ_c separates the AF phase and the random-singlet phase [66], while in the kagome model it is estimated to be $\Delta_c \simeq 0.4$ where Δ_c separates the randomness-irrelevant QSL phase (e.g., the Z_2 spin-liquid phase) and the randomness-relevant random-singlet phase [67].

In the present paper, we employ the exact diagonalization (ED) method in computing various physical quantities. The ED method is precise and is applicable even to systems with frustration, while it has a disadvantage of being limited to very small system sizes. In our computation, the total number of spins N is $N = 12,18,24,30$ for $T = 0$ and $N = 12,18$ for $T > 0$, periodic boundary conditions being employed. Sample average is taken over 100 ($N = 12,18,24$) and 50 ($N = 30$) independent bond realization in the $T = 0$ calculation, while 100 ($N = 12$) and 30 ($N = 18$) in the $T > 0$ calculation in both cases of the triangular and the kagome models. The shape of the lattice is illustrated in Figs. 14 and 15 in Appendix B for

the triangular and the kagome lattices, respectively. In what follows, the energy and temperature are normalized in units of J.

III. RESULTS I: THE TRIANGULAR LATTICE

In this section, we study the ground-state and the finite-temperature properties of the random-bond $S = 1/2$ AF Heisenberg model on the triangular lattice. We begin with the sublattice magnetization associated with the three-sublattice 120° structure. The sublattice magnetization per spin m_s may be defined by

$$m_s^2 = \frac{1}{3}\sum_{\alpha}\left[\left\langle \frac{1}{(N/6)(N/6+1)}\left(\sum_{i\in\alpha}\mathbf{S}_i\right)^2\right\rangle\right] = \frac{12}{N(N+6)}\sum_{\alpha}\left[\sum_{i,j\in\alpha}\langle \mathbf{S}_i\cdot\mathbf{S}_j\rangle\right], \quad (2)$$

where $\alpha = 1,2,3$ denotes three triangular sublattices of the original triangular lattice, and the sum $i \in \alpha (i,j \in \alpha)$ is taken over all sites i (i and j) belonging to the αth sublattice. The symbol $\langle\cdots\rangle$ denotes the thermal average, and $[\cdots]$ the average over the bond disorder. Note that m_s is normalized to give unity for the classical, perfectly ordered 120° structure.

We also define the rescaled sublattice magnetization per spin $\tilde{m}_s$ by subtracting the auto-correlated part as

$$\tilde{m}_s^2 = m_s^2 - \frac{12N}{N(N+6)}\frac{3}{4}. \quad (3)$$

The subtraction of the autocorrelated part is made so that the sublattice magnetization tends to zero at $T \to \infty$ even for finite N. In the thermodynamic limit $N \to \infty$,$\tilde{m}_s$ approaches m_s at any temperature.

In Fig. 1, we show the temperature dependence of the rescaled sublattice magnetization per spin, $\tilde{m}_s$, for $N = 12$ and 18 for several values of the randomness Δ. In the regular and weakly random cases, $\tilde{m}_s$ increases monotonically with decreasing the temperature, and eventually saturates. This increase of m_s at finite temperature is associated with the growth of the AF short-range order. When the randomness

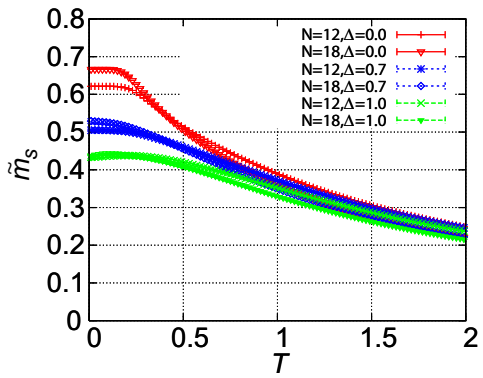

FIG. 1. (Color online) The temperature dependence of the rescaled sublattice magnetization per spin $\tilde{m}_s$ of the triangular-lattice Heisenberg antiferromagnet for the randomness $\Delta = 0$, 0.7, and 1.0 and for the sizes $N = 12$ and 18. The definition of $\tilde{m}_s$ is given in the text.

gets stronger, $\tilde{m}_s$ is suppressed as a result of the suppression of the AF short-range order due to the randomness.

An interesting observation is that, for the strongest randomness $\Delta = 1$,$\tilde{m}_s$ tends to *decrease* weakly with decreasing the temperature in the lower temperature range of $T \lesssim 0.2$, exhibiting some sort of crossover. This suppression is weak, but tends to be more eminent for larger sizes. Such suppression of the AF short-range order is compatible with the formation of the random-singlet-type state at $T \lesssim 0.2$. Similar suppression was also reported in Ref. [66] in the temperature dependence of $1/T_1$ in the similar temperature and size range. There, Z_2 vortex [75] was invoked to be a possible candidate of this crossoverlike anomaly, since the suppression was observed only for lattices larger than $N = 18$. Further study is required to clarify the nature of this crossover phenomenon, which is observed only for modestly large systems with strong randomness.

In order to get further information about the static spin correlations of the model, we investigate the static spin structure factor $S(\mathbf{q})$ defined by

$$S(\mathbf{q}) = \frac{1}{N}\left[\left\langle\left|\sum_j \mathbf{S}_j e^{i\mathbf{q}\cdot\mathbf{R}_j}\right|^2\right\rangle\right], \quad (4)$$

where $\langle\cdots\rangle$ means the ground-state expectation, $\mathbf{q}$ is the wave vector, and $\mathbf{R}_j$ is the position vector at the site j. The computed static spin structure factor at $T = 0$ is shown in Fig. 2 as

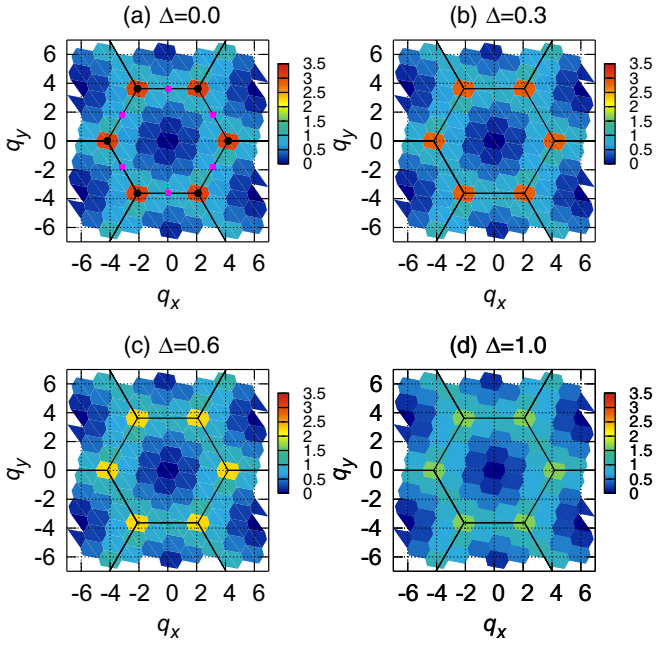

FIG. 2. (Color online) Intensity plots of the static spin structure factors $S(\mathbf{q})$ of the triangular-lattice Heisenberg antiferromagnet in the wave vector (q_x,q_y) plane for several values of the randomness $\Delta = 0$ (a), 0.3 (b), 0.6 (c), and 1.0 (d). The lattice constant $a = 1$ is the nearest-neighbor distance of the triangular lattice. The system size is $N = 30$. The solid black line depicts the first Brillouin zone of triangular lattice. Each small hexagon corresponds to the resolution unit, and the center of each distorted hexagon is the wave-vector point we can treat in $N = 30$ system. The black point in (a) represents the K point, while the purple point the M point: see the text for details.

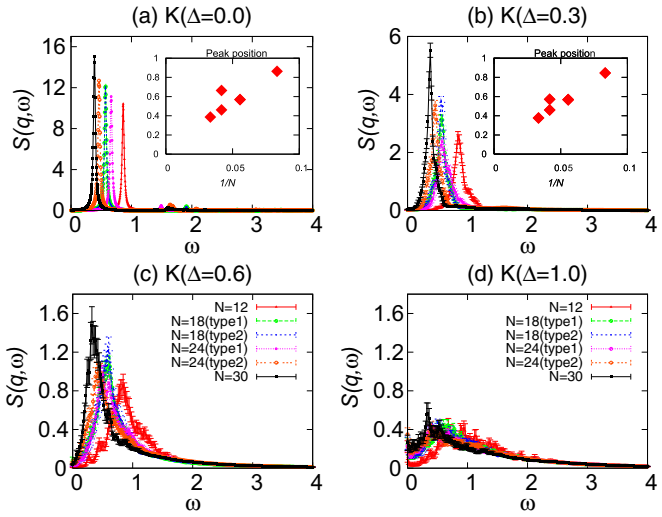

FIG. 3. (Color online) The ω dependence of the dynamical structure factors of the triangular-lattice Heisenberg antiferromagnet taken at the K point, $\mathbf{q} = (\pm 2\pi/3, \pm 2\pi/\sqrt{3})$ and $(\pm 4\pi/3, 0)$, for several values of the randomness $\Delta = 0$ (a), 0.3 (b), 0.6 (c), and 1.0 (d). The critical randomness separating the AF state and the random-singlet state is $\Delta_c \simeq 0.6$. Note the difference in the ordinate scale between (a) and (b)–(d). In the inset of (a) and (b), the ω value of the dominant peak is plotted vs the inverse system size $1/N$.

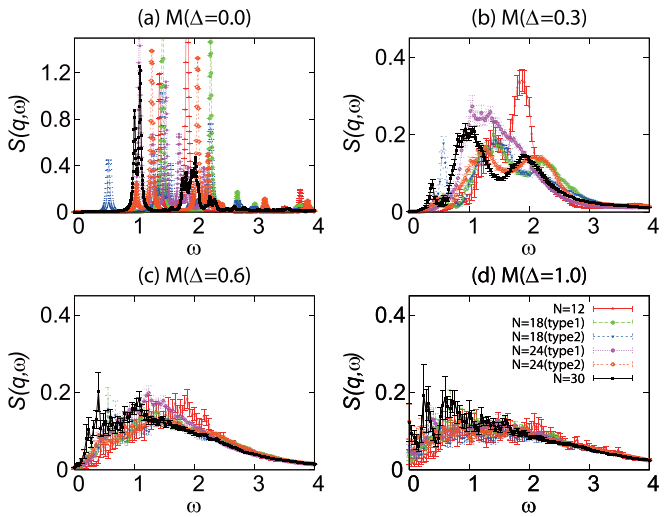

FIG. 4. (Color online) The ω dependence of the dynamical structure factors of the triangular-lattice Heisenberg antiferromagnet taken at the M point, $\mathbf{q} = (0, \pm 2\pi/\sqrt{3})$ and $(\pm\pi, \pm\pi/\sqrt{3})$, for several values of the randomness $\Delta = 0$ (a), 0.3 (b), 0.6 (c), and 1.0 (d). The critical randomness separating the AF state and the random-singlet state is estimated to be $\Delta_c \simeq 0.6$. Note the difference in the ordinate scale between (a) and (b)–(d), and between this figure and Fig. 3.

an intensity plot in the wave-vector (q_x, q_y) plane for several values of the randomness, $\Delta = 0$ (a), 0.3 (b), 0.6 (c), and 1.0 (d). The system size is $N = 30$.

Although the resolution is rather low due to the small system size, several characteristic features are clearly discernible from the figure. In the regular case $\Delta = 0$, eminent peaks corresponding to the AF LRO are observed at the so-called K points, $\mathbf{q} = (q_x, q_y) = (\pm 2\pi/3, \pm 2\pi/\sqrt{3})$ and $(\pm 4\pi/3, 0)$, where the length unit is taken as the nearest-neighbor distnace of the triangular lattice. As the randomness gets stronger, the peak at the K points is gradually suppressed. The AF LRO is expected to vanish for $\Delta > \Delta_c \simeq 0.6$ [66]. Such a phase-transition-like sharp change of behavior around $\Delta_c \sim 0.6$, however, is not necessarily clear here, presumably due to the small system size of $N = 30$. In fact, a rounded peak persists at the K point even at the maximal randomness of $\Delta = 1$, suggesting the persistence of the AF short-range order in the random-singlet state. Thus, in the triangular case, the random-singlet state coexists with the AF *short-range* order.

In order to get further information about the dynamical spin correlations of the model, we next investigate the dynamical spin structure factor defined by

$$S(\mathbf{q},\omega) = \sum_n \left[\left| \langle \psi_n | S^z_q | \psi_0 \rangle \right|^2 \delta\left(\omega - (E_n - E_0)\right) \right], \qquad (5)$$

where $S^z_{\mathbf{q}}$ is the z component of the Fourier transform of the spin operator, ψ_n is the eigenfunction of the Hamiltonian (1) whose eigenvalue is E_n, and ψ_0 is the ground-state eigenfunction with the eigenvalue E_0. By using the continued fraction method [76], it may be rewritten as

$$S(\mathbf{q},\omega) = -\lim_{\eta\to 0} \frac{1}{\pi} \mathrm{Im} \left[\langle \psi_0 | \left(S^z_q\right)^\dagger \frac{1}{\omega + E_0 - \mathcal{H} + i\eta} S^z_q | \psi_0 \rangle \right]$$

$$= -\lim_{\eta\to 0} \frac{1}{\pi} \mathrm{Im} \left[\frac{\langle \psi_0 | \left(S^z_q\right)^\dagger S^z_q | \psi_0 \rangle}{\omega + E_0 + i\eta - a_0 - \cfrac{b_1^2}{z - a_1 - \cfrac{b_2^2}{z - a_2 - \cdots}}} \right], \qquad (6)$$

where a_i and b_{i+1} are the diagonal and subdiagonal elements of the tridiagonal Hamiltonian obtained by the Lanczos method. In implementing the continued-fraction expansion, we performed at least 1000 iterations. A small but finite $\eta, \eta = 0.02$, is used.

The ω dependence of $S(\mathbf{q},\omega)$ computed at the K point is shown in Fig. 3, while the one at the M point, which is located at the midpoints of the first Brillouin zone (BZ) edges, i.e., $\mathbf{q} = (0, \pm 2\pi/\sqrt{3})$ and $(\pm\pi, \pm\pi/\sqrt{3})$, is in Fig. 4. The randomness Δ is taken to be $\Delta = 0$ (a), 0.3 (b), 0.6 (c), and 1.0 (d). Note the difference in the ordinate scale between Figs. 3 and 4, and between (a) and (b)–(d) panels.

Reflecting the AF short-range order of the triangular model, the $S(\mathbf{q},\omega)$ intensity tends to be larger at the K point (Fig. 3) than at the M point (Fig. 4) irrespective of the Δ value. The contrast between the K and the M points, however, tends to be milder for larger Δ.

In the regular case $\Delta = 0$, the dominant peak observed in $S(\mathbf{q},\omega)$ at the K point [Fig. 3(a)] is a single magnon excitation. Indeed, the peak location in ω tends to zero when N is increased toward the thermodynamic limit. Similar behavior is observed also in the weakly random case of $\Delta = 0.3$: see the insets of Figs. 3(a) and 3(b). As shown in Fig. 4(a), several peaks are observed at the M point. According to the recent

spin-wave analysis for the regular model, $S(\mathbf{q},\omega)$ at the M point exhibits a leading peak at $\omega \simeq 0.8$ [77]. Indeed, if one looks at our data of $\Delta = 0$ for $N = 24$ and 30, the dominant peak appears at a nearby position $\omega \simeq 1$.

As the randomness becomes stronger getting into the random-singlet phase, $S(\mathbf{q},\omega)$ exhibit less peaky behavior both at the K and the M points. As can be seen from Figs. 4(c) and 4(d), it exhibits a broad distribution extending to higher ω, with a finite intensity gradually growing at $\omega = 0$. This demonstrates that the random-singlet state of the triangular model is indeed magnetically gapless both at the K and M points. The observed gapless feature of $S(\mathbf{q},\omega)$ is fully consistent with the gapless behavior observed in several other observables in Ref. [66]. While the intensity tends to be larger at the K point than at the M point, the difference tends to be smaller for larger Δ as in the case of the static spin structure factor.

In the random-singlet state, $S(\mathbf{q},\omega)$ exhibits a tail in ω in the higher-ω range. The asymptotic ω dependence of this tail is found to be exponential $\approx \exp[-\omega/\omega_0]$ with a characteristic energy scale ω_0. Estimates of ω_0 yields a value around $2 \sim 2.5$.

IV. RESULTS II: THE KAGOME LATTICE

Next, we deal with the random-bond $S = 1/2$ AF Heisenberg model on the kagome lattice whose Hamiltonian is given by Eq. (1). We first examine the temperature dependence of the two representative types of the rescaled sublattice magnetization per spin, $\tilde{m}_s$, each associated with the $q = 0$ and the $\sqrt{3} \times \sqrt{3}$ structures. As in the triangular case, it is normalized to give unity for the classical, perfectly ordered $q = 0$ or $\sqrt{3} \times \sqrt{3}$ structure, while the autocorrelated part is subtracted. The temperature dependence of the computed $\tilde{m}_s$ is shown in Fig. 5 for $N = 18$ for several values of the randomness Δ.

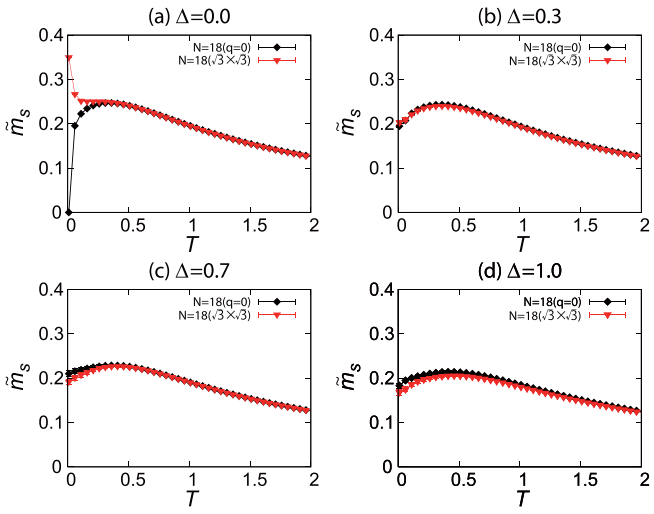

FIG. 5. (Color online) The temperature dependence of the rescaled sublattice magnetization per spin, $\tilde{m}_s$, associated with the $q = 0$ and $\sqrt{3} \times \sqrt{3}$ orders of the kagome-lattice Heisenberg antiferromagnet for several values of the randomness $\Delta = 0$ (a), 0.4 (b), 0.7 (c), and 1.0 (d).

Numerically, it has been established that the regular model exhibits neither the $q = 0$ nor the $\sqrt{3} \times \sqrt{3}$ LRO even at $T = 0$ [8]. These AF orders are not realized in the random model, either [67]. Yet, the temperature and the size dependence of $\tilde{m}_s$ is expected to provide us useful information about the associated AF short-range order.

For the regular model, while the spin-wave-type $1/S$ expansion suggested the possible dominance of the $\sqrt{3} \times \sqrt{3}$ order [78,79], the recent numerical results from the exact-diagonalization [13] and the DMRG [12] calculations suggested the dominance of the $q = 0$ state. Though our present data for $N = 30$ apparently suggest the dominance of the $\sqrt{3} \times \sqrt{3}$ short-range order, our maximum size $N = 30$ is smaller than the ones of Refs. [13] and [12], i.e., $N = 36$ and 108, respectively, and might be subject to stronger finite-site effect. In any case, as the randomness gets stronger, the difference between the $q = 0$ order and the $\sqrt{3} \times \sqrt{3}$ order tends to be negligible.

To get further information about the spin correlations of the model, we compute the $T = 0$ static spin structure factor, and the results for $N = 30$ are shown in Fig. 6 as an intensity plot in the (q_x,q_y) plane for the randomness of $\Delta = 0$ (a), 0.4 (b), 0.7 (c), and 1.0 (d). The length unit here is taken to be the nearest-neighbor distance of the original kagome lattice.

In the regular case shown in Fig. 6(a), the intensity appears primarily along the zone boundary of the extended BZ, consistently with the behavior reported in Refs. [12,13]. We note that the recent numerical studies for larger system of $N = 36$ reveal additional small peaks at the wave vectors

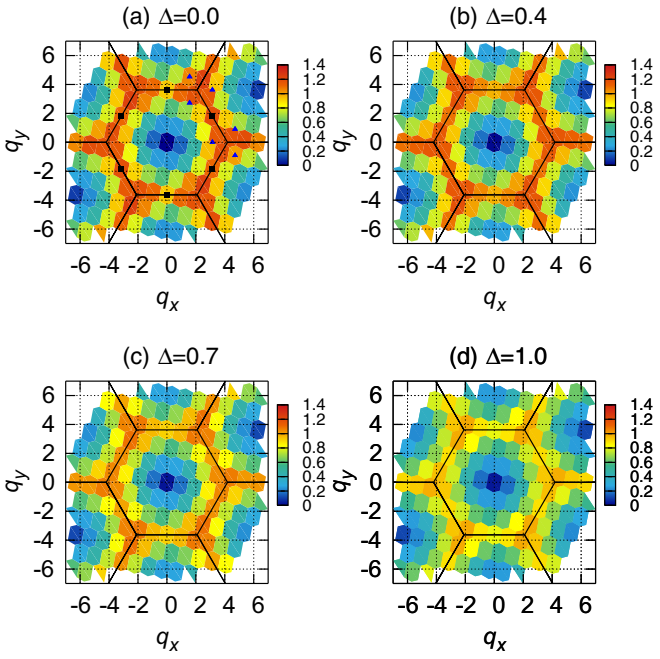

FIG. 6. (Color online) Intensity plots of the static spin structure factors $S(\mathbf{q})$ of the kagome-lattice Heisenberg antiferromagnet in the wave-vector (q_x,q_y) plane for several values of the randomness $\Delta = 0$ (a), 0.4 (b), 0.7 (c), and 1.0 (d). The lattice constant $a = 1$ is the nearest-neighbor distance of the kagome lattice. The system size is $N = 30$. The solid black line depicts the zone boundary of the extended BZ. The black square in (a) represents the Γ point, while the blue triangle represents the M point.

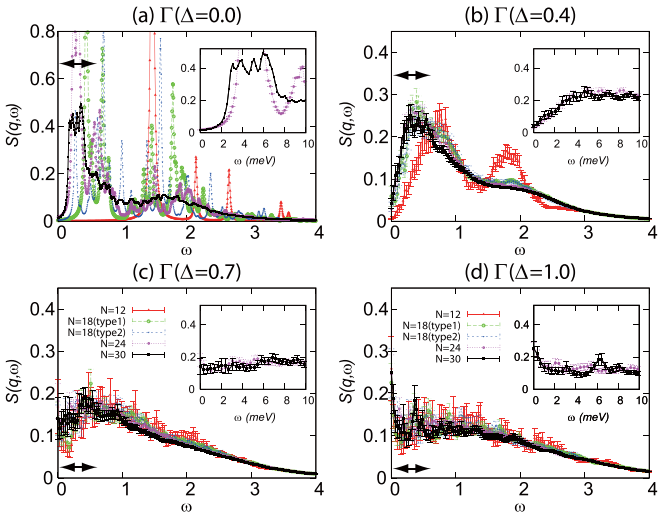

FIG. 7. (Color online) The ω dependence of the dynamical spin structure factor $S(\mathbf{q},\omega)$ of the kagome-lattice Heisenberg antiferromagnet taken at the Γ point, $\mathbf{q} = (0,\pm 2\pi/\sqrt{3})$ and $(\pm\pi,\pm\pi/\sqrt{3})$, for several values of the randomness $\Delta = 0$ (a), 0.3 (b), 0.6 (c), and 1.0 (d). The critical randomness separating the randomness-irrelevant QSL state and the random-singlet state is estimated to be $\Delta_c \simeq 0.4$. The insets are magnified views of the low-ω region in units of meV, where $J = 17$ meV is assumed with herbertsmithite in mind. Note the difference in the ordinate scale between (a) and (b)–(d).

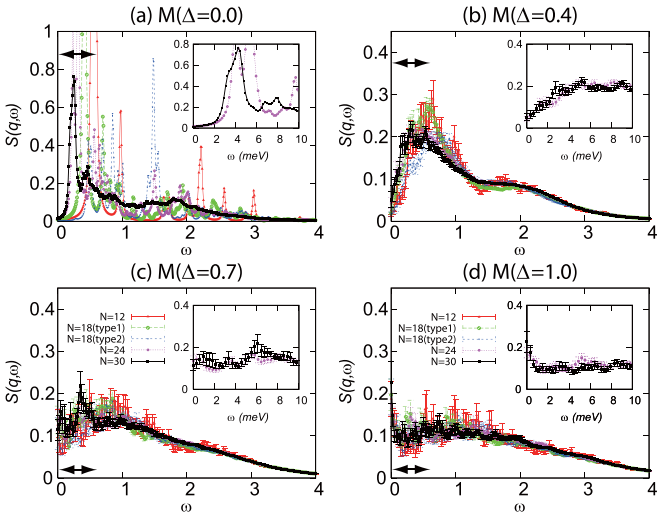

FIG. 8. (Color online) The ω dependence of the dynamical spin structure factor $S(\mathbf{q},\omega)$ of the kagome-lattice Heisenberg antiferromagnet taken at the M point, $\mathbf{q} = (0,\pm\pi/\sqrt{3})$ and $(\pm\pi/2,\pm\pi/2\sqrt{3})$, for several values of the randomness $\Delta = 0$ (a), 0.3 (b), 0.6 (c), and 1.0 (d). The critical randomness separating the randomness-irrelevant QSL state and the random-singlet state is estimated to be $\Delta_c \simeq 0.4$. The insets are magnified views of the low-ω region in units of meV, where $J = 17$ meV is assumed with herbertsmithite in mind. Note the difference in the ordinate scale between (a) and (b)–(d).

corresponding to the $q = 0$ state, $\mathbf{q} = (0,\pm 2\pi/\sqrt{3})$ and $(\pm\pi,\pm\pi/\sqrt{3})$, which are located along the zone boundary of the extended BZ [12,13], although this peak is not clearly discernible in our present data of $N = 30$. As can be seen from Figs. 6(a)–6(d), qualitative features of $S(\mathbf{q})$ do not change much even when the randomness is introduced up to $\Delta = 1$, except that the ridgelike intensity along the extended BZ boundary is somewhat broadend.

We also compute the dynamical spin structure factor $S(\mathbf{q},\omega)$ at the two representative wave vectors, i.e., the so-called Γ point, $\mathbf{q} = (0,\pm 2\pi/\sqrt{3})$ and $(\pm\pi,\pm\pi/\sqrt{3})$, and the M point, $\mathbf{q} = (0,\pm\pi/\sqrt{3})$ and $(\pm\pi/2,\pm\pi/2\sqrt{3})$. The computed ω dependence of $S(\mathbf{q},\omega)$ is shown for several values of the randomness Δ in Fig. 7 for the Γ point, and in Fig. 8 for the M point. The ω dependence of the dynamical spin structure factor shows some differences between in the randomness-irrelevant QSL state at $\Delta < \Delta_c$ and in the randomness-relevant QSL state at $\Delta > \Delta_c$. In contrast to the case of the triangular model, $S(\mathbf{q},\omega)$ exhibits a rather broad distribution even in the regular case, yet with some pronounced peaks remaining both at the Γ and the M points as shown in Figs. 7(a) and 8(a). Although our data of $N \leqslant 30$ are still subject to considerable finite-size effects, Läuchli *et al.* reported that $S(\mathbf{q},\omega)$ for $N = 24$ and for larger $N = 36$ came close, suggesting that $S(\mathbf{q},\omega)$ for $N = 30$ were not far from that of the bulk system. The issue of a small nonzero gap exists or not in the regular systems is beyond the capability of our present calculation.

For larger $\Delta > \Delta_c \simeq 0.4$ corresponding to the random-singlet state, by contrast, $S(\mathbf{q},\omega)$ exhibits both at the Γ and M points a nearly flat distribution in the wide ω range of, say, $\omega \lesssim 1.5$ and extends to higher ω, with a nonzero intensity growing at $\omega = 0$. This demonstrates the gapless nature of excitations in the random-singlet state both for the Γ and M points. In the case of the strongest randomness $\Delta = 1.0$, even an $\omega = 0$ peak appears at both Γ and M points. As can be seen from Figs. 7(d) and 8(d), the overall behavior of $S(\mathbf{q},\omega)$ are very much similar at the Γ and the M points in the random-singlet state.

In the random-singlet state, $S(\mathbf{q},\omega)$ exhibits a tail in ω in the higher-ω range both at the Γ and M points. The asymptotic ω dependence of this tail is found to be exponential, $\approx 9\exp[-\omega/\omega_0]$, with a characteristic energy scale ω_0. In the kagome model, such an exponential tail is also realized even in the regular system. Estimates of ω_0 yields a value around $1.5 \sim 2$, slightly increasing with increasing the randomness Δ.

The behavior of $S(\mathbf{q},\omega)$ in the random-singlet state of the kagome model is rather similar to the one of the triangular model shown in Figs. 3 and 4. One difference might be that $S(\mathbf{q},\omega)$ in the low-energy region is even more flatter in the kagome model, and the $\omega = 0$ peak is more eminent.

Anyway, the gapless behavior with an almost flat distribution extending to higher ω irrespective of the q value is a common feature of the observed dynamical structure factor of both the triangular and the kagome models for larger Δ, and might be regarded as a characteristic of the random-singlet state.

In order to make comparison with the recent inelastic neutron-scattering data on a single-crystal of herbertsmithite [64], we provide in the insets of Figs. 7 and 8 their low-energy part of the experimental data, which corresponds to the range indicated by the arrow in the main panel. Since the experimental data now available are limited to the low-energy region of $\omega \lesssim 10$ meV, we show in the inset exactly this range, i.e., $\omega < 10$ meV, by using an experimental estimate of $J \simeq 17$ meV. This estimate of the exchange

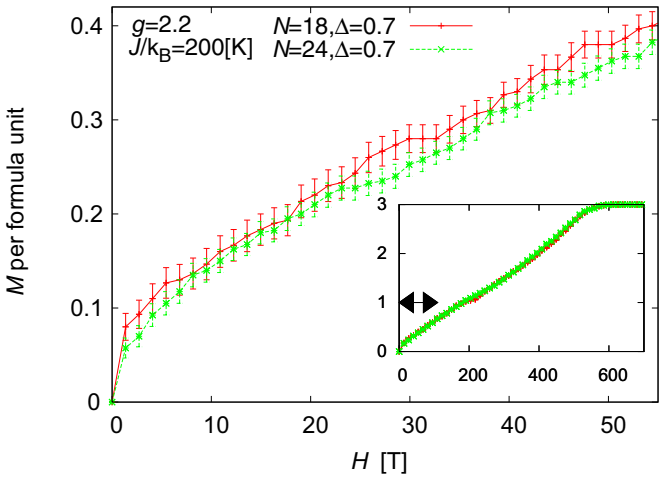

FIG. 9. (Color online) The $T = 0$ magnetization curve for the randomness of $\Delta = 0.7$ for $N = 18$ and 24, in the wider field range (inset) and in the lower field range (main panel) corresponding to the region indicated by the arrow in the inset. With herbertsmithite in mind, the magnetization M is normalized per formula unit of herbertsmithite, i.e., the saturation value taken to be 3, while an applied field is given in units of tesla with assuming the experimental g factor ($g \simeq 2.2$) and J value ($J \simeq 200$ K) of herbertsmithite [65].

coupling J of herbertsmithite is made via neutron-scattering measurements on powder samples [59]. On comparison with the corresponding experimental data (Fig. 2 of Ref. [64]), one finds a nice agreement especially for the strong randomness $\Delta = 1$ shown in panel (d), including the features of (1) a plateaulike behavior observed for $2 \lesssim \omega \lesssim 10$ meV, (2) an $\omega = 0$ peak observed at $\omega \lesssim 1.5$ meV without any gap, and (3) the insensitivity of the overall behavior of $S(\mathbf{q},\omega)$ on the wave vector $\mathbf{q}$. We emphasize that the data of the random model shown in panel (d) appears to resemble the experimental one much more than that of the nonrandom system of panel (a). This observation certainly lends support to the view that the randomness is playing a significant role in the QSL state of herbertsmithite.

Very good agreement with experiment is also found for the magnetization curve. In Fig. 9, we show the ground-state magnetization curve for the randomness $\Delta = 0.7$ for $N = 18$ and 24, where the magnetization M is normalized per formula unit of herbertsmithite, i.e., the saturation value taken to be 3, while an applied field is given in units of tesla with assuming the experimental g factor ($g \simeq 2.2$) and J value ($J \simeq 200$ K) of herbertsmithite [65]. Then, the computed magnetization curve of Fig. 9 indeed exhibits an almost quantitative agreement with the recent experimental data given in Fig. 2 of Ref. [65] in the same units.

Two features might be noticed. One is the absence of any plateaulike anomaly in the magnetization curve. As shown in the inset, it exhibits a near linear behavior in an entire region of H up to the near saturation, except for some "wavy" behavior occurring at intermediate fields (which becomes less visible for the stronger randomness of $\Delta = 1$ [67]). As reported Ref. [67], we have found that the plateaulike anomaly tends to go away for $\Delta > \Delta_c$, yielding a near linear behavior. The other notable feature of the magnetization curve might be an upper-convex gapless behavior observed at weaker fields near $H = 0$. This enhanced behavior of the low-field magnetization is consistent with the Curie-like behavior of the susceptibility observed for stronger randomness [67], and is likely to be borne by the "free" or "almost free" spins inevitably generated in the random-single state.

V. SUMMARY AND DISCUSSION

We studied by means of an ED method the nature of spin correlations of the random-bond $S = 1/2$ AF Heisenberg models on the triangular and the kagome lattices via the static and the dynamical spin structure factors. To highlight the possible importance of frustration, we also made a comparative calculation for the unfrustrated random-bond $S = 1/2$ AF Heisenberg model on the square lattice.

Both the triangular and the kagome models exhibit the randomness-induced QSL behavior when the randomness exceeds a critical value as observed in previous studies, while the unfrustrated square model persistently exhibits the AF LRO up to the maximal randomness without showing the QSL behavior. This demonstrates that the frustration is certainly playing a role in stabilizing the random-singlet state.

The random-singlet states in the triangular and the kagome models have some similarities, but also some differences. The random singlet state of the both models exhibit gapless behaviors, dependent on the wave vector $\mathbf{q}$ only weakly, while the dynamical spin structure factor $S(\mathbf{q},\omega)$ exhibit a broad distribution in ω extending to higher ω with an exponential tail. Especially in the strongly random kagome model, $S(\mathbf{q},\omega)$ hardly depends on $\mathbf{q}$ and exhibits an almost flat distribution for a wide range of ω with a $\omega = 0$ peak.

As discussed in Sec. IV, our results for the dynamical spin structure factor for the strongly random kagome model compares quite favorably with the recent inelastic neutron-scattering data on the kagome herbertsmithite, including (1) a plateaulike behavior observed for $2 \lesssim \omega \lesssim 10$ meV, (2) an $\omega = 0$ peak observed $\omega \lesssim 1.5$ meV without any gap, and (3) the insensitivity on the wave vector $\mathbf{q}$. Since the present experimental data are limited to the low-energy range $\omega \lesssim 10$ meV, it would be interesting to perform further experiments in the higher-energy range of $\omega \gtrsim 10$ meV to make further comparison. In addition, the computed magnetization curve is found to exhibit a good, almost quantitative agreement with the recent experimental data on herbertsmithite.

In making a truly quantitative comparison with the experimental data on herbertsmithite, ones needs to examine several effects not considered in the present model, i.e., the effect of the Dzyaloshinskii-Moriya interaction and the triangular layer between the kagome layers, etc. How the results depend or do not depend on the particular form of the randomness needs further clarification. In particular, the possible effect of the dilution-type randomness pointed out experimentally in Refs. [60,61,63] and studied theoretically in Ref. [73] might be incorporated.

An important open theoretical question in the kagome model might be the distinction and the true relation between the observed two types of QSL-like states, i.e., the randomness-irrelevant QSL state realized at $\Delta < \Delta_c$ and the randomness-relevant QSL state (random-singlet state) realized at $\Delta > \Delta_c$.

One intuitive view of this transition (or crossover) occurring at $\Delta \simeq \Delta_c$ might be that singlet states tend to exhibit an Anderson localization there. The enhanced flat feature of $S(\mathbf{q},\omega)$ observed in the random singlet state at $\Delta > \Delta_c$ is certainly consistent with such a picture. In this view, the randomness-irrelevant QSL state is an extended RVB-like state, while the randomness-relevant QSL state is an Anderson-localized state of singlets. Whether this naive picture captures correct physics behind the two types of QSL-like states needs further clarification.

In contrast to the kagome case, the neutron-scattering data are not presently availabe for triangular organic salts due to the organic nature of the material. Another route to the random-singlet state of $S = 1/2$ triangular AFs might be an insulating mixed crystal $Cs_2Cu(Br_{1-x}Cl_x)_4$. Experiments suggest that this compound might exhibit a nonmagnetic ground state in the range $x > 0.17$ [80], at which the system possesses a considerable amount of randomness associated with the random arrangement of Cl^- and Br^-. Interestingly, in this QSL-like regime, the gapless behavior including the T-linear low-temperature specific heat is observed [81]. It might be interesting to perform neutron-scattering measurements on this compound in its QSL regime to make a comparison with our present data.

The naive picture of the random singlet state, which is observed in common with the triangular and the kagome models, might be that tightly bound spin singlets are preferentially formed at stronger J_{ij} bonds, leaving loosely bound spin singlets or nearly free spins at weaker J_{ij} bonds. Of course, such simple assignment of singlets to randomly distributed J_{ij} bonds immediately meets contradiction or 'frustration', revealing that the singlet formation in the spatially random environment is not a trivial matter at all. A subtle balance between the potential energy due to the local energy gain arising from the nonuniform J_{ij} and the kinetic energy arising from the resonance of the local singlet states should determine the true ground state. In fact, in both cases of the triangular and the kagome models, we have observed that, although there generally exists a tendency that the strong singlet with larger negative $\mathbf{S}_i \cdot \mathbf{S}_j$ value tends to be formed at strong bonds with large J_{ij} value, this tendency is quite often violated in the sense that strong local singlet is sometimes formed at weaker bonds, or the singlet formation remains weak even at stronger bonds.

In summary, we investigated the nature of spin correlations in the randomness-induced QSL-like state, the random-singlet state, of the random-bond $S = 1/2$ AF Heisneberg model on the triangular and the kagome lattices by computing their static and dynamical spin structure factors by means of the exact diagonalization method. Gapless behaviors accompanied by the broad distribution extending to higher energy, dependent on the wave vector only weakly, is observed in the dynamical spin structure factor $S(\mathbf{q},\omega)$ in the random-singlet states of the both models in common. Especially in the kagome case with strong randomness, $S(\mathbf{q},\omega)$ hardly depends on the wave vector $\mathbf{q}$ and exhibits an almost flat distribution in a wide range of ω, accompanied by the $\omega = 0$ peak. These features agree with the recent inelastic-neutron scattering data on a single-crystal herbertsmithite semiquantitatively, suggesting that the QSL state observed in herbertsmithite is indeed the random-induced QSL state, i.e., the random-singlet state.

ACKNOWLEDGMENTS

The authors are thankful to K. Kanoda, H. Tanaka, I. Ono, C. Hotta, T. Sakai and K. Hiji for useful discussion. H. Tanaka pointed the possible importance of the Jahn-Teller distortion associated with the Cu^{2+} in the triangular layer in assigning the quenched randomness in the exchange interaction of herbertsmithite. The ED calculation was performed by use of TITPACK version 2. The QMC calculation was carried out using the ALPS QMC application [83]. They are thankful to ISSP, the University of Tokyo for providing us with CPU time. This study is supported by a Grant-in-Aid for Scientific Research No. 25247064. One of the authors (T.S.) acknowledges the financial support from the Mochizuki Fund of Yukawa Memorial Foundation.

APPENDIX A

In this Appendix, as a typical model of unfrustrated $S = 1/2$ random systems, we deal with the random-bond $S = 1/2$ AF Heisenberg model on the square lattice. The Hamiltonian is given by Eq. (1), the random interaction J_{ij} obeying the uniform distribution characterized by the randomness parameter Δ, commonly with the triangular and the kagome cases. The ED study on the bond-randomness effect in the unfrustrated square model have already been made in Ref. [82]. It was shown there that, in the square-lattice case, the sublattice magnetization survived against the bond randomness. In this appendix, we show not only the ground-state sublattice magnetization but also the temperature dependence of the sublattice magnetization, together with the static and the dynamical ground-state spin structure factors, in order to make full comparison with the corresponding data for the frustrated systems.

The lattice size is $N = 8,10,16,18,20,24$, and 32 with periodic boundary conditions in all directions. The sample average is performed for 300 ($N = 8,10$), 200 ($N = 16,18$), 100 ($N = 20,24$), and 5 ($N = 32$) independent bond realizations in calculating the sublattice magnetization, and for 100 ($N < 32$) and 20 ($N = 32$) independent bond realizations in calculating the static and the dynamical spin structure factors.

The size dependence of the $T = 0$ squared sublattice magnetization per spin, m_s^2, is shown in Fig. 10 for various randomness Δ. The sublattice magnetization here is the one

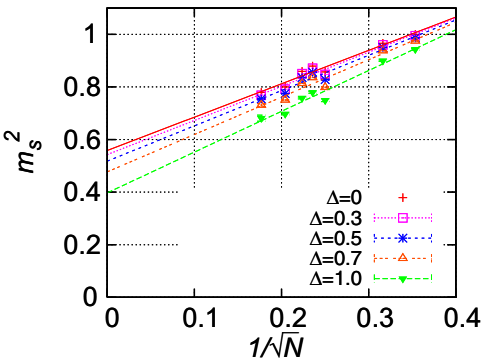

FIG. 10. (Color online) The rescaled $T = 0$ squared sublattice magnetization per spin, m_s^2, of the square-lattice Heisenberg antiferromagnet plotted vs $1/\sqrt{N}$ (N the lattice size) for several values of the randomness Δ.

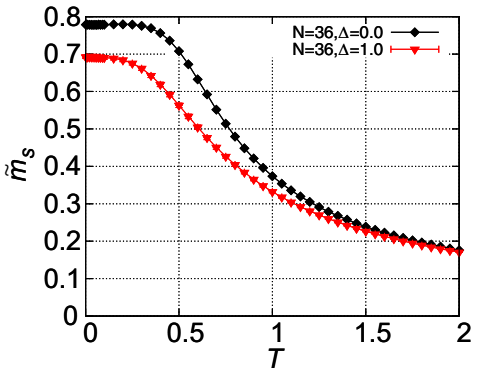

FIG. 11. (Color online) The temperature dependence of the rescaled sublattice magnetization per spin, $\tilde{m}_s$, of the square-lattice Heisenberg antiferromagnet for the size $N = 36$, and for the randomness $\Delta = 0$ and 1.0.

associated with the two-sublattice AF order. As can clearly be seen from the figure, m_s remains nonzero even in the thermodynamic limit for all values of Δ, indicating that the AF LRO persists up to the maximal randomness of $\Delta = 1$ as reported in Ref. [82]. This is in sharp contrast to the cases of the triangular and the kagome models where the AF LRO gives way to the random-singlet state for sufficiently strong randomness. Hence, not only the randomness but also the frustration plays a significant role in stabilizing the random-singlet state. In other words, all three elements, i.e., the strong quantum fluctuation, the frustration, and the quenched randomness, conspire to realize the present QSL state, the random-singlet state.

In Fig. 11, we show the temperature dependence of the rescaled sublattice magnetization per spin, $\tilde{m}_s$, for the regular $\Delta = 0$ and for the maximally random $\Delta = 1$ cases. The lattice size is $N = 36$. The calculation here is made by use of the quantum Monte Carlo method [83], which is possible due to the absence of frustration in the square-lattice model. In both the regular and the maximally random cases, $\tilde{m}_s$ increases monotonically with decreasing the temperature down to the lowest temperature studied, as can be seen from Fig. 11. In particular, in contrast to the maximally random $\Delta = 1$ case of the triangular model and the general case of the kagome model,

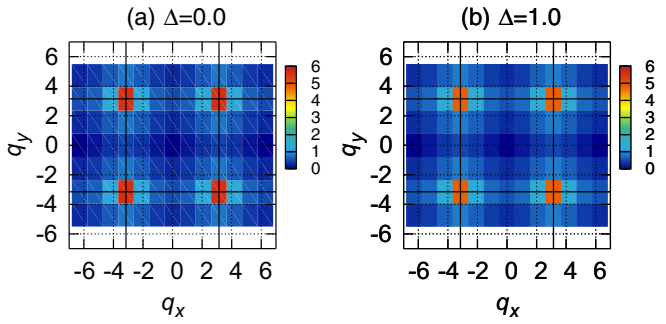

FIG. 12. (Color online) Intensity plots of the $T = 0$ static spin structure factor $S(\mathbf{q})$ of the square-lattice Heisenberg antiferromagnet in the wave-vector (q_x, q_y) plane for the randomness $\Delta = 0$ (a), and 1 (b). The solid black line represents the zone boundary of the first BZ of the square lattice.

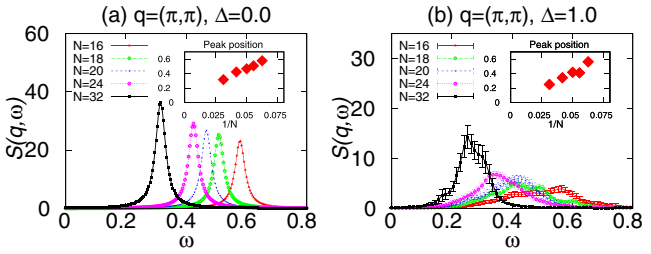

FIG. 13. (Color online) The ω dependence of the $T = 0$ dynamical spin structure factor $S(\mathbf{q},\omega)$ of the square-lattice antiferromagnet taken at the wave vector $\mathbf{q} = (\pi,\pi)$ for the randomness $\Delta = 0$ (a) and 1 (b).

the crossover behavior associated with a decrease of $\tilde{m}_s$ in the lower-temperature regime is not observed in the square model even in the maximally random case. This suggests that the crossover behavior observed in the triangular and the kagome models might be a characteristic of the formation of the QSL-like state including the random-singlet state.

The $T = 0$ static spin structure factor $S(\mathbf{q})$ is shown in Fig. 12 as an intensity plot in the wave-vector plane. The lattice size is $N = 24$. The computed $S(\mathbf{q})$ exhibit rather sharp peaks at $\mathbf{q} = (\pm\pi,\pm\pi)$ corresponding to the AF LRO of the model both for $\Delta = 0$ and $\Delta = 1$. In fact, overall $S(\mathbf{q})$ looks quite similar between the regular case of $\Delta = 0$ (a) and the maximal random case of $\Delta = 1$ (b).

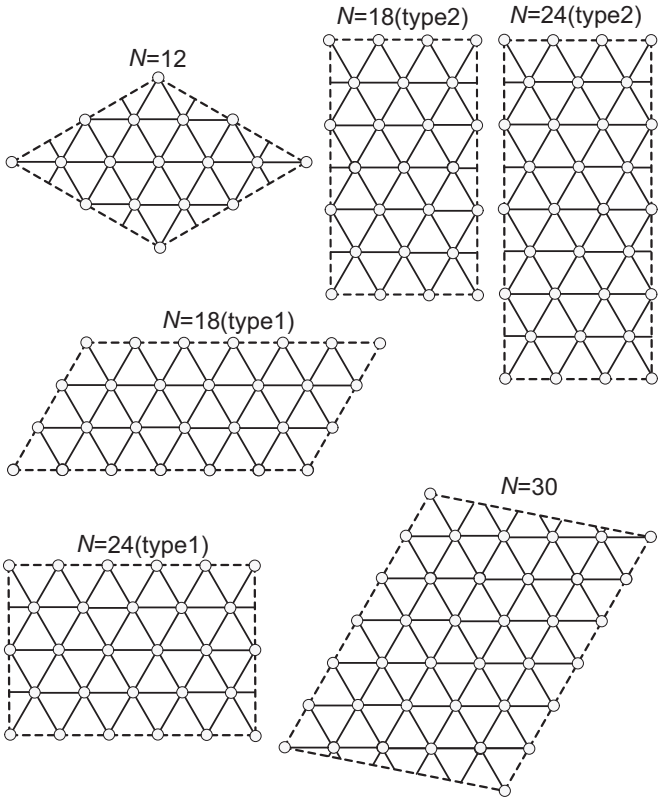

FIG. 14. The lattice shapes used in the exact diagonalization calculation of the triangular-lattice model for various N. Periodic boundary conditions are applied in all directions.

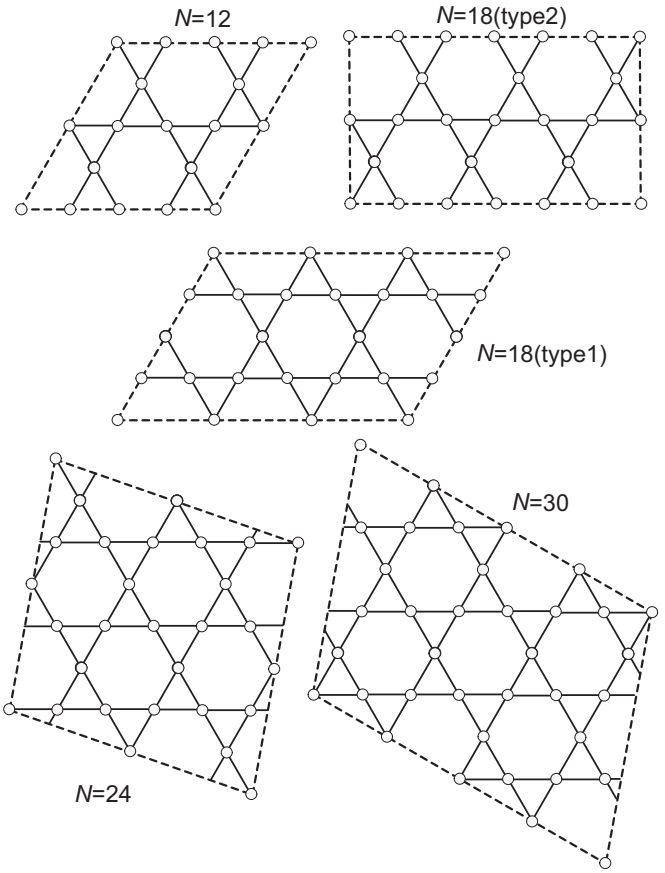

FIG. 15. The lattice shapes used in the exact diagonalization calculation of the kagome-lattice model for various N. Periodic boundary conditions are applied in all directions.

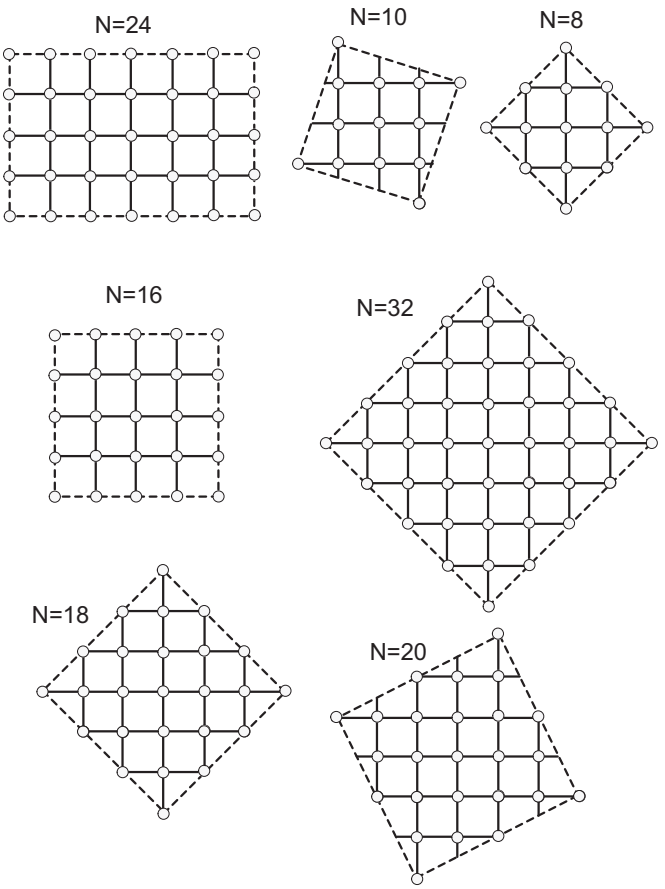

FIG. 16. The lattice shapes used in the exact diagonalization calculation of the square-lattice model for various N. Periodic boundary conditions are applied in all directions.

The ω dependence of the dynamical spin structure factor $S(\mathbf{q},\omega)$ at a wave vector $\mathbf{q} = (\pi,\pi)$ corresponding to the AF order is shown in Fig. 13 for the randomness $\Delta = 0$ (a) and for 1 (b). The dominant peak is a single magnon excitation, the peak location tending to zero toward the thermodynamic limit as shown in the insets. As in the static case, $S(\mathbf{q},\omega)$ looks qualitatively similar between the regular and the maximally random cases, while the magnon peak becomes broader in the random case.

APPENDIX B

In this Appendix, we show the lattice shapes used in our ED calculation for various lattice sizes N. The cases of the triangular, kagome, and square lattices are given in Figs. 14–16, respectively. In all cases, periodic boundary conditions are applied in all directions.

[1] P. W. Anderson, Mater. Res. Bull. **8**, 153 (1973).
[2] B. Bernu, P. Lecheminant, C. Lhuillier, and L. Pierre, Phys. Rev. B **50**, 10048 (1994).
[3] L. Capriotti, A. E. Trumper, and S. Sorella, Phys. Rev. Lett. **82**, 3899 (1999).
[4] S. R. White and A. L. Chernyshev, Phys. Rev. Lett. **99**, 127004 (2007).
[5] V. Elser, Phys. Rev. Lett. **62**, 2405 (1989).
[6] R. R. P. Singh and D. A. Huse, Phys. Rev. Lett. **68**, 1766 (1992).
[7] P. W. Leung and V. Elser, Phys. Rev. B **47**, 5459 (1993).
[8] P. Lecheminant, B. Bernu, C. Lhuillier, L. Pierre, and P. Sindzingre, Phys. Rev. B **56**, 2521 (1997).
[9] Ch. Waldtmann, H.-U. Everts, B. Bernu, C. Lhuillier, P. Sindzingre, P. Lecheminant, and L. Pierre, Eur. Phys. J. B **2**, 501 (1998).
[10] G. Misguich and B. Bernu, Phys. Rev. B **71**, 014417 (2005).
[11] R. R. P. Singh and D. A. Huse, Phys. Rev. B **76**, 180407 (2007); **77**, 144415 (2008).
[12] H. C. Jiang, Z. Y. Weng, and D. N. Sheng, Phys. Rev. Lett. **101**, 117203 (2008).
[13] A. M. Läuchli and C. Lhuillier, arXiv:0901.1065.
[14] P. Sindzingre and C. Lhuillier, Europhys. Lett. **88**, 27009 (2009).
[15] H. Nakano and T. Sakai, J. Phys. Soc. Jpn. **80**, 053704 (2011).

[16] A. M. Lauchli, J. Sudan, and E. S. Sorensen, Phys. Rev. B **83**, 212401 (2011).
[17] S. Yan, D. A. Huse, and S. R. White, Science **332**, 1173 (2011).
[18] S. Depenbrock, I. P. McCulloch, and U. Schollwock, Phys. Rev. Lett. **109**, 067201 (2012).
[19] S. Sugiura and A. Shimizu, Phys. Rev. Lett. **111**, 010401 (2013).
[20] S. Nishimoto, N. Shibata, and C. Hotta, Nat. Commun. **4**, 2287 (2013).
[21] H. Nakano and T. Sakai, J. Phys. Soc. Jpn. **83**, 104710 (2014).
[22] S. Sachdev, Phys. Rev. B **45**, 12377 (1992).
[23] Y.-M. Lu, Y. Ran, and P. A. Lee, Phys. Rev. B **83**, 224413 (2011).
[24] M. B. Hastings, Phys. Rev. B **63**, 014413 (2000).
[25] Y. Ran, M. Hermele, P. A. Lee, and X.-G. Wen, Phys. Rev. Lett. **98**, 117205 (2007).
[26] Y. Iqbal, F. Becca, and D. Poilblanc, Phys. Rev. B **84**, 020407(R) (2011).
[27] Y. Iqbal, F. Becca, S. Sorella, and D. Poilblanc, Phys. Rev. B **87**, 060405(R) (2013).
[28] L. Messio, B. Bernu, and C. Lhuillier, Phys. Rev. Lett. **108**, 207204 (2012).
[29] J. B. Marston and C. Zeng, J. Appl. Phys. **69**, 5962 (1991).
[30] G. Evenbly and G. Vidal, Phys. Rev. Lett. **104**, 187203 (2010).
[31] Y. Shimizu, K. Miyagawa, K. Kanoda, M. Maesato, and G. Saito, Phys. Rev. Lett. **91**, 107001 (2003).
[32] Y. Kurosaki, Y. Shimizu, K. Miyagawa, K. Kanoda, and G. Saito, Phys. Rev. Lett. **95**, 177001 (2005).
[33] Y. Shimizu, K. Miyagawa, K. Kanoda, M. Maesato, and G. Saito, Phys. Rev. B **73**, 140407(R) (2006).
[34] S. Ohira, Y. Shimizu, K. Kanoda, and G. Saito, J. Low Temp. Phys. **142**, 153 (2006).
[35] S. Yamashita, Y. Nakazawa, M. Oguni, Y. Oshima, H. Nojiri, Y. Shimizu, K. Miyagawa, and K. Kanoda, Nat. Phys. **4**, 459 (2008).
[36] M. Yamashita, N. Nakata, Y. Kasahara, T. Sasaki, N. Yoneyama, N. Kobayashi, S. Fujimoto, T. Shibauchi, and Y. Matsuda, Nat. Phys. **5**, 44 (2009).
[37] R. S. Manna, M. de Souza, A. Brühl, J. A. Schlueter, and M. Lang, Phys. Rev. Lett. **104**, 016403 (2010).
[38] M. Abdel-Jawad, I. Terasaki, T. Sasaki, N. Yoneyama, N. Kobayashi, Y. Uesu, and C. Hotta, Phys. Rev. B **82**, 125119 (2010).
[39] F. L. Pratt, P. J. Baker, S. J. Blundell, T. Lancaster, S. Ohira-Kawamura, C. Baines, Y. Shimizu, K. Kanoda, I. Watanabe, and G. Saito, Nature (London) **471**, 612 (2011).
[40] M. Poirier, S. Parent, A. Côté, K. Miyagawa, K. Kanoda, and Y. Shimizu, Phys. Rev. B **85**, 134444 (2012).
[41] K. Sedlmeier, S. Elsässer, D. Neubauer, R. Beyer, D. Wu, T. Ivek, S. Tomić, J. A. Schlueter, and M. Dressel, Phys. Rev. B **86**, 245103 (2012).
[42] S. Nakajima, T. Suzuki, T. Ishii, K. Ohishi, I. Watanabe, T. Goto, A. Oosawa, N. Yoneyama, N. Kobayashi, F. L. Pratt, and T. Sasaki, J. Phys. Soc. Jpn. **81**, 063706 (2012).
[43] K. Itoh, H. Itoh, M. Naka, S. Saito, I. Hosako, N. Yoneyama, S. Ishihara, T. Sasaki, and S. Iwai, Phys. Rev. Lett. **110**, 106401 (2013).
[44] T. Itou, A. Oyamada, S. Maegawa, M. Tamura, and R. Kato, Phys. Rev. B **77**, 104413 (2008).
[45] T. Itou, A. Oyamada, S. Maegawa, and R. Kato, Nat. Phys. **6**, 673 (2010).
[46] M. Yamashita, N. Nakata, Y. Senshu, M. Nagata, H. M. Yamamoto, R. Kato, T. Shibauchi, and Y. Matsuda, Science **328**, 1246 (2010).
[47] S. Yamashita, T. Yamamoto, Y. Nakazawa, M. Tamura, and R. Kato, Nat. Commun. **2**, 275 (2011).
[48] D. Watanabe, M. Yamashita, S. Tonegawa, Y. Oshima, H. M. Yamamoto, R. Kato, I. Sheikin, K. Behnia, T. Terashima, S. Uji, T. Shibauchi, and Y. Matsuda, Nat. Commun. **3**, 1090 (2012).
[49] M. Abdel-Jawad, N. Tajima, R. Kato, and I. Terasaki, Phys. Rev. B **88**, 075139 (2013).
[50] W. LiMing, G. Misguich, P. Sindzingre, and C. Lhuillier, Phys. Rev. B **62**, 6372 (2000).
[51] H. Morita, S. Watanabe, and M. Imada, J. Phys. Soc. Jpn. **71**, 2109 (2002).
[52] O. I. Motrunich, Phys. Rev. B **72**, 045105 (2005).
[53] S.-S. Lee and P. A. Lee, Phys. Rev. Lett. **95**, 036403 (2005).
[54] S. Yunoki and S. Sorella, Phys. Rev. B **74**, 014408 (2006).
[55] S.-S. Lee, P. A. Lee, and T. Senthil, Phys. Rev. Lett. **98**, 067006 (2007).
[56] Y. Qi, C. Xu, and S. Sachdev, Phys. Rev. Lett. **102**, 176401 (2009).
[57] L. F. Tocchio, A. Parola, C. Gros, and F. Becca, Phys. Rev. B **80**, 064419 (2009).
[58] M. P. Shores, E. A. Nytko, B. M. Bartlett, and D. G. Nocera, J. Am. Chem. Soc. **127**, 13462 (2005).
[59] J. S. Helton, K. Matan, M. P. Shores, E. A. Nytko, B. M. Bartlett, Y. Yoshida, Y. Takano, A. Suslov, Y. Qiu, J.-H. Chung, D. G. Nocera, and Y. S. Lee, Phys. Rev. Lett. **98**, 107204 (2007).
[60] M. A. de Vries, K. V. Kamenev, W. A. Kockelmann, J. Sanchez-Benitez, and A. Harrison, Phys. Rev. Lett. **100**, 157205 (2008).
[61] P. Mendelse and F. Bert, J. Phys. Soc. Jpn. **79**, 011001 (2010).
[62] J. S. Helton, K. Matan, M. P. Shores, E. A. Nytko, B. M. Bartlett, Y. Qiu, D. G. Nocera, and Y. S. Lee, Phys. Rev. Lett. **104**, 147201 (2010).
[63] D. E. Freedman, T. H. Han, A. Prodi, P. Müller, Q.-Z. Huan, Y.-S. Chen, S. M. Webb, Y. S. Lee, T. M. McQueen, and D. G. Nocera, J. Am. Chem. Soc. **132**, 16185 (2010).
[64] T.-H. Han, J. S. Helton, S. Chu, D. G. Nocera, J. A. Rodriguez-Rivera, C. Broholm, and Y. S. Lee, Nature (London) **492**, 406 (2012).
[65] T.-H. Han, R. Chisnell, C. J. Bonnoit, D. E. Freedman, V. S. Zapf, N. Harrison, D. G. Nocera, Y. Takano, and Y. S. Lee, arXiv:1402.2693.
[66] K. Watanabe, H. Kawamura, H. Nakano, and T. Sakai, J. Phys. Soc. Jpn. **83**, 034714 (2014).
[67] H. Kawamura, K. Watanabe, and T. Shimokawa, J. Phys. Soc. Jpn. **83**, 103704 (2014).
[68] C. Dasgupta and S.-K. Ma, Phys. Rev. B **22**, 1305 (1980).
[69] R. N. Bhatt and P. A. Lee, Phys. Rev. Lett. **48**, 344 (1982).
[70] D. S. Fisher, Phys. Rev. B **50**, 3799 (1994).
[71] Y.-C. Lin, R. Mélin, H. Rieger and F. Iglói, Phys. Rev. B **68**, 024424 (2003).
[72] M. Tarzia and G. Biroli, Europhys. Lett. **82**, 67008 (2008).
[73] R. R. P. Singh, Phys. Rev. Lett. **104**, 177203 (2010).
[74] H. Tanaka (private communication).
[75] H. Kawamura and S. Miyashita, J. Phys. Soc. Jpn. **53**, 4138 (1984).

[76] E. R. Gagliano and C. A. Balseiro, Phys. Rev. Lett. **59**, 2999 (1987).
[77] M. Mourigal, W. T. Fuhrman, A. L. Chernyshev, and M. E. Zhitomirsky, Phys. Rev. B **88**, 094407 (2013).
[78] A. Chubukov, Phys. Rev. Lett. **69**, 832 (1992).
[79] A. L. Chernyshev and M. E. Zhitomirsky, Phys. Rev. Lett. **113**, 237202 (2014).
[80] T. Ono, H. Tanaka, T. Nakagomi, O. Kolomiyets, H. Mitamura, F. Ishikawa, T. Goto, K. Nakajima, A. Oosawa, Y. Koike, K. Kakurai, J. Klenke, P. Smeibidle, M. Meissner and H. Aruga Kaori, J. Phys. Soc. Jpn. Suppl. **74**, 135 (2005).
[81] T. Ono (parivate communication).
[82] N. Laflorencie, S. Wessel, A. Lauchli, and H. Rieger, Phys. Rev. B **73**, 060403(R) (2006).
[83] A. F. Albuquerque, F. Alet, P. Corboz, P. Dayal, A. Feiguin, L. Gamper, E. Gull, S. Gurtler, A. Honecker, R. Igarashi, M. Korner, A. Kozhevnikov, A. Lauchli, S. R. Manmana, M. Matsumoto, I. P. McCulloch, F. Michel, R. M. Noack, G. Pawlowski, L. Pollet, T. Pruschke, U. Schollwock, S. Todo, S. Trebst, M. Troyer, P. Werner, and S. Wessel, J. Magn. Magn. Mater. **310**, 1187 (2007), see also http://alps.comp-phys.org.